

Unveiling Rabi dynamics through angle-resolved photoelectron momentum distributions using an ω - 2ω pulse pair

Yi-Jia Mao ¹, Hong-Bin Yao ^{1,2}, Mingrui He,³ Zhao-Han Zhang,¹ Yang Li,^{1,*} and Feng He^{1,4}

¹Key Laboratory for Laser Plasmas (Ministry of Education) and School of Physics and Astronomy, Collaborative Innovation Center for IFSA (CICIFSA), Shanghai Jiao Tong University, Shanghai 200240, China

²Key Laboratory of New Energy and Materials Research of Xinjiang Education Department, Xinjiang Institute of Engineering, Urumqi 830091, China

³Department of Basic Courses, Naval University of Engineering, Wuhan 430033, China

⁴CAS Center for Excellence in Ultra-intense Laser Science, Shanghai 201800, China



(Received 27 September 2023; accepted 2 November 2023; published 22 November 2023)

We present an interferometric method for studying the Rabi dynamics in atoms by employing an ω - 2ω extreme ultraviolet pulse pair generated from the seeded free-electron laser. By solving the time-dependent Schrödinger equation (TDSE) for hydrogen atoms, we study the photoelectron spectrum that emerges when the ω pulse triggers Rabi oscillations between the ground state and the first excited state. The interference between the one-photon and two-photon ionization pathways in the photoelectron signal gives access to the phase difference between the one- and two-photon transition amplitudes. Compared to the cases without Rabi oscillations, an additional π phase jump is observed in the energy domain. Based on perturbation theory, we demonstrate that this phase jump directly reflects the ultrafast buildup of Rabi oscillations in the time domain. The present ω - 2ω scheme can be generalized and applied to other more complex atoms or molecules provided that the populations of bound states can be efficiently and coherently modulated using the free-electron laser.

DOI: [10.1103/PhysRevA.108.053117](https://doi.org/10.1103/PhysRevA.108.053117)

I. INTRODUCTION

Rabi oscillations are the periodic population flopping of two states when an external field with a resonant frequency is applied [1–5]. They have long been a topic of interest due to their unique features and prominent applications in the coherent control of quantum systems [6–11]. For instance, Rabi oscillations of excitons in single quantum dots allow for the coherent control of the quantum state of single excitons [12]. By utilizing the Freeman resonance, a scheme is proposed to drive two-photon Rabi oscillations to Rydberg states. This scheme paves the way for the manipulation of Rydberg states [6]. In the context of strong field ionization, high-order above-threshold ionization of atoms from a coherent superposition of bound states is studied, emphasizing how the relative amplitude and phase of these states can be controlled with a weak resonant laser pulse and how the photoelectron spectra are affected by the relative phase [13]. In stretching molecules, the Rabi oscillations, which depend on bond length and involve nuclear motions, enable the control of strong-field dissociation of molecules [14,15].

Aulter-Townes (AT) splitting is often regarded as observable evidence of Rabi dynamics [16]. In the near-infrared regime, which is often associated with the coupling between excited states or multiphoton resonance, the splitting can be observed in the attosecond transient absorption spectrum (ATAS) [17–22]. When the infrared laser can simultaneously

induce tunneling ionization, the doublet can be extended to every order in high harmonic generation (HHG) spectroscopy [23].

In the short-wavelength domain, the AT splitting can be observed in the photoelectron energy spectrum (PES) [24–27]. However, most of the studies remain theoretical due to limitations in the experimental setups. In the past few decades, the development of the free-electron laser (FEL) technique has advanced the study of ionization processes in atoms or molecules in the extreme-ultraviolet (XUV) or even soft x-ray regimes [28–30]. If the pulses are from self-amplified spontaneous emission (SASE) FEL sources, they are usually unable to drive Rabi oscillations due to the significant change on a shot-to-shot basis. However, they can still be applied in the preparation of excited states [6,31]. Seeded FEL, such as Free Electron Laser Radiation for Multidisciplinary Investigations (FERMI), can generate XUV pulses for coherent control and detection of light-matter interactions. This is possible due to its high reproducibility in temporal and spatial properties [32,33]. By using this technique, an asymmetric AT doublet is observed in the measured photoelectron spectrum of helium atoms. The AT doublet is attributed to the Rabi dynamics between the ground state and an excited state [31]. The result is later reproduced by solving the time-dependent Schrödinger equation (TDSE) and a minimal three-state model [34]. The influence of the quantum interference effect between resonant and nonresonant photoionization pathways, as well as the ac-Stark shift effect, is addressed in relation to the ultrafast buildup of the asymmetric doublet structure. Recently, a feasible experimental scheme was proposed to detect the

*liyang22@sjtu.edu.cn

fingerprint of Rabi oscillations in the superfluorescence spectrum [35].

A further application of seeded FEL is to produce ω - 2ω pulse pairs at the XUV or soft x-ray regimes with a tunable time delay and high coherence. With the assistance of accelerator physics, the relative phase of the fundamental wavelength and its second harmonic can be adjusted with attosecond precision [33,36]. The absolute phase can be extracted from the photoelectron angular distribution (PAD) by analyzing the interference of different partial waves [37]. With a complete characterization of the pulse pairs, this method has been employed to extract the angle-resolved phase difference between the one-photon and two-photon ionization pathways in neon [38]. In the presence of intermediate resonant states, an additional phase shift of the two-photon pathways can be inferred, with the one-photon pathway serving as the reference. The energy derivative of the phase difference corresponds to the Wigner time delay difference of the partial waves [39], which offers a perspective for measuring the time of photon absorption. Many theoretical calculations have also been conducted to study the left-right asymmetry in this case for different atom systems [40–43]. When the pulse pair is long enough to trigger the Rabi oscillation between the two resonant states, the extracted phases can be strongly modulated. In this case, both the information of the population flopping and the phase shifts induced by the Rabi oscillation could be encoded in the PAD. To our best understanding, this has not yet been studied before.

In this work, we propose a scheme to study the Rabi dynamics in atoms using an ω - 2ω pulse pair. By numerically solving the TDSE, we obtain the PADs for both ω - 2ω pulse pairs, with and without Rabi oscillations, in hydrogen atoms. The phase difference between the one- and two-photon ionization pathways can be determined from the PAD. Compared to the cases without Rabi oscillations, we observe that Rabi oscillations exhibit an additional π phase jump in the energy-dependent phase difference. It is a consequence of both the population oscillation between the two resonant states and the corresponding phase shifts. In addition, the phase information is examined for various pulse widths to evaluate the phase difference characteristics at different stages of Rabi oscillations. Rabi oscillations with near-resonant frequencies are also considered for the generalization of this method.

This paper is organized as follows. Section II presents the numerical methods used in this paper. These methods include solving the TDSE and extracting the phase information from the PAD. In Sec. III, the phase difference is extracted for both cases: with and without Rabi oscillations, respectively. The processes involving different numbers of Rabi periods or near-resonant frequencies are also analyzed. Section IV provides a summary of the paper. Atomic units are applied throughout the paper unless otherwise specified.

II. NUMERICAL METHODS

A. TDSE simulation

We numerically solve the TDSE for hydrogen atoms irradiated by a pair of XUV pulses. All the simulations are performed using the publicly available QPC-TDSE program

[44]. In the velocity gauge, the TDSE is written as

$$i \frac{\partial \psi(\mathbf{r}, t)}{\partial t} = \left[-\frac{1}{2} \nabla^2 - i\mathbf{A}(t) \cdot \nabla + \frac{1}{r} \right] \psi(\mathbf{r}, t), \quad (1)$$

with the vector potential of the two-color field in the dipole approximation in the form

$$\begin{aligned} \mathbf{A}(t) = & A_\omega \exp\left(-2 \ln 2 \frac{t^2}{\tau^2}\right) \sin(\omega t) \mathbf{e}_z \\ & + A_{2\omega} \exp\left(-2 \ln 2 \frac{t^2}{\tau^2}\right) \sin(2\omega t - \delta) \mathbf{e}_z, \end{aligned} \quad (2)$$

where ω is the fundamental angular frequency of the pulse pair, A_ω and $A_{2\omega}$ are the amplitudes of the ω and 2ω components, respectively, τ is the full width at half maximum (FWHM), and δ is the relative phase between the two components of the pulse pair. In the calculation, we smoothly truncate the tails of the Gaussian envelope to avoid any unphysical effects.

Since only linearly polarized fields are applied, the magnetic quantum number is constant and set to zero. Then Eq. (1) is solved by expanding the wave function via B-spline functions $B_n(r)$ and spherical harmonics $Y_{l0}(\theta, \phi)$

$$\psi(\mathbf{r}, t) = \frac{1}{r} \sum_{nl} c_{nl}(t) B_n(r) Y_{l0}(\theta, \phi). \quad (3)$$

Here, the summation involves 5000 active radial B-spline bases and 30 angular spherical harmonic bases. Eighth-order B-spline functions are defined on a knot sequence that is linearly spaced in the radial direction. For the time propagation, the Crank-Nicholson propagator is utilized with a time step size of $\Delta t = 0.008$ a.u. The simulation is conducted in a spherical box with a radius of $R_m = 1800$ a.u. The absorbing boundary is located at $R_a = 1750$ a.u. A mask function in the form $\cos^\alpha[\pi(r - R_a)/2(R_m - R_a)]$ is applied at the boundary with $\alpha = 0.002$. We verified that all the results are converged in terms of spatial and temporal discretization.

The ground state of the hydrogen atom is obtained by diagonalizing the field-free Hamiltonian. At the end of the laser pulse, the angle-resolved photoelectron momentum distribution (PMD) is calculated by projecting the final wave function onto the field-free Coulomb continuum states. For each momentum $\mathbf{k} = (k, \theta, \phi)$ in spherical coordinates, the momentum distribution detected at infinity can be expressed as [45,46]

$$P(\mathbf{k}) = |\langle \psi_{\mathbf{k}}^- | \psi_{t_f} \rangle|^2, \quad (4)$$

where $\psi_{\mathbf{k}}^-$ is the scattering state for momentum \mathbf{k} at infinity with incoming boundary condition [47], t_f is the time when the laser field vanishes. The calculation in QPC is realized by first evaluating the partial wave PMD

$$P_{l0}(k) = \sqrt{\frac{2}{\pi}} \sum_n c_{nl}(t_f) I_{ln}(k), \quad (5)$$

where

$$I_{ln} = k^{-1} \int_0^{R_m} w_l(kr) B_n(r) dr. \quad (6)$$

$w_l(kr)$ is the regular solution to

$$\frac{d^2 w}{d\rho^2} + \left\{ 1 - \frac{l(l+1)}{\rho^2} - \frac{2}{\rho k} \right\} w = 0. \quad (7)$$

Then the angle-resolved PMD, which is a collection of PADs with different k , can be calculated as

$$I(k, \theta, \phi) = \left| \sum_l (-i)^l e^{i\Delta_l(k)} Y_{l0}(\theta, \phi) P_{l0}(k) \right|^2, \quad (8)$$

where

$$\Delta_l(k) = \arg \left[\Gamma \left(l + 1 - \frac{i}{k} \right) \right], \quad (9)$$

is the Coulomb phase shift [48].

B. Phase extraction from photoelectron spectra

It is known that photoionization by $\omega-2\omega$ shows no interference in the angle-integrated PES [40,49,50]. On the contrary, the PAD is a coherent sum of various partial waves. As a result, for electrons initially located at s orbitals, the PADs for each momentum k after $\omega-2\omega$ photoionization contain the s , p , and d partial waves. These PADs can be expressed as [37,38]

$$I(\theta) = \left| c_s e^{i\sigma_{sd}} Y_{00}(\theta, \phi) - c_p e^{i\sigma_{pd} + i(\delta - \pi/2)} Y_{10}(\theta, \phi) - c_d Y_{20}(\theta, \phi) \right|^2, \quad (10)$$

where $\sigma_{sd} = \sigma_s - \sigma_d$ and $\sigma_{pd} = \sigma_p - \sigma_d$. c_s , c_p , and c_d are the partial wave amplitudes of s , p , and d waves, respectively. σ_s , σ_p , and σ_d are the partial wave phases, which include the Coulomb phase shift but exclude the prefactor $-\pi/2$. The prefactor corresponds to the centrifugal potential phase of $(-i)^l$ in Eq. (8). Since the maximum l for $Y_{l0}(\theta, \phi)$ in Eq. (10) is 2, $I(\theta)$ can be expanded through Legendre polynomials up to the fourth order as

$$I(\theta) \propto 1 + \sum_{l=1}^4 \beta_l P_l(\cos \theta). \quad (11)$$

The β parameters in Eq. (11) can be calculated as [37,38]

$$\beta_1 = \frac{2\sqrt{3}[2\sqrt{5}c_p c_d \sin(\sigma_{pd} + \delta) - 5c_p c_s \sin(\sigma_{ps} + \delta)]}{5(c_s^2 + c_p^2 + c_d^2)}, \quad (12)$$

$$\beta_2 = \frac{2(5c_d^2 + 7c_p^2 - 7\sqrt{5}c_d c_s \cos \sigma_{sd})}{7(c_s^2 + c_p^2 + c_d^2)}, \quad (13)$$

$$\beta_3 = \frac{6\sqrt{15}c_p c_d \sin(\sigma_{pd} + \delta)}{5(c_s^2 + c_p^2 + c_d^2)}, \quad (14)$$

$$\beta_4 = \frac{18c_d^2}{7(c_s^2 + c_p^2 + c_d^2)}, \quad (15)$$

$$\beta_1 - \frac{2}{3}\beta_3 = -\frac{2\sqrt{3}c_p c_s \sin(\sigma_{ps} + \delta)}{c_s^2 + c_p^2 + c_d^2}, \quad (16)$$

where $\sigma_{ps} = \sigma_{pd} - \sigma_{sd}$. In this way, the δ dependence of the PAD is transmitted to the dependence of the β parameters. The odd-order β_1 and β_3 oscillate sinusoidally with the relative phase δ , while the even-order β_2 and β_4 are independent of δ . As a result, we can extract the phase of the two-photon

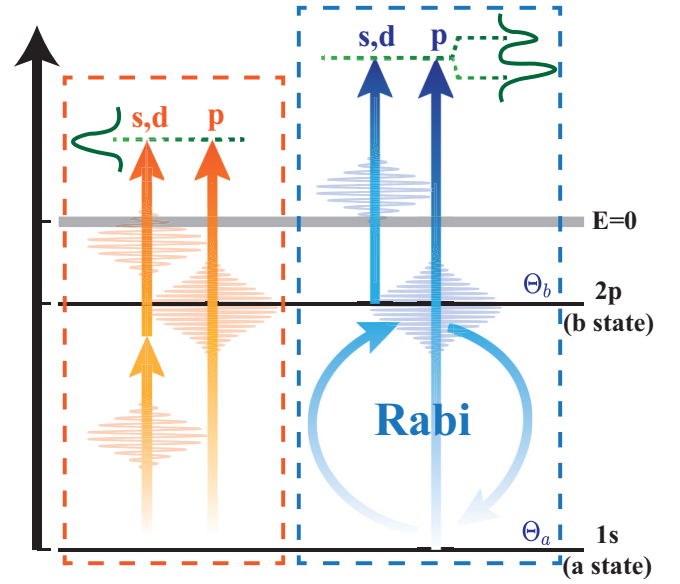


FIG. 1. The sketch of the interferometric method for photoionization of hydrogen atoms by $\omega-2\omega$ pulse pairs. The orange pulse pair on the left corresponds to the nonresonant case with $\omega = 0.35$ a.u. The blue one on the right refers to the resonant case with $\omega = 0.375$ a.u. The Rabi oscillation occurs between the $1s$ and $2p$ states, as indicated by the curved arrows. For the sake of convenience, the $1s$ and $2p$ states are labeled as states $|\psi_a\rangle$ and $|\psi_b\rangle$, respectively. $\Theta_a(t)$ and $\Theta_b(t)$ are additional phases induced by Rabi dynamics for states $|\psi_a\rangle$ and $|\psi_b\rangle$.

ionization pathway relative to the one-photon ionization one, namely, σ_{ps} and σ_{pd} , by fitting the β parameters with respect to δ .

III. RESULTS AND DISCUSSION

Figure 1 illustrates the sketch of the interferometric method for photoionization of hydrogen atoms by $\omega-2\omega$ pulse pairs. In the nonresonant case, where the intermediate resonance is absent, the $1s$ electron can be ionized either to the s and d waves by absorbing two ω photons, or alternatively to the p wave by absorbing one 2ω photon. The different partial waves will interfere with each other in the angle-resolved PMD. If the intensity of the pulse pair is not too strong, the depletion of the population as well as the Stark energy shift of the initial state can be safely neglected. Then, the interference between the one-photon and two-photon ionization amplitudes is trivial and can be well explained by conventional perturbation theory. When the ω pulse is tuned to the resonance of the ground state $1s$ and the first excited state $2p$, Rabi oscillations will occur if the pulse duration is long enough. This will result in an AT doublet in the PES [16]. In addition to the AT splitting, we demonstrate here that the signature of the Rabi oscillations will be mapped to the phases of different partial waves. It is well known that Rabi oscillations will lead to population flopping between the two states $|\psi_a\rangle$ and $|\psi_b\rangle$. Defining $\tilde{a}(t)$ and $\tilde{b}(t)$ as the complex amplitudes of the two resonant states. Their phases, $\Theta_a(t)$ and $\Theta_b(t)$, are generally nonzero when Rabi oscillations occur. In the $\omega-2\omega$ photoionization process, the one-photon ionization is affected by the amplitude and

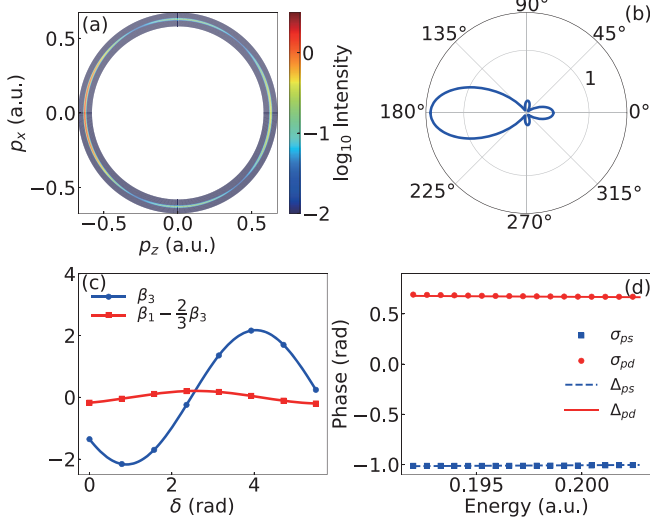


FIG. 2. (a) The PMD for the ω - 2ω pair with $\omega = 0.35$ a.u., $I_\omega = 1 \times 10^{13}$ W/cm 2 , $I_{2\omega} = 2.3 \times 10^{11}$ W/cm 2 , $\delta = 0$, and $\tau = 15.1$ fs. (b) The PAD at $E = 0.2$ a.u. (c) Extracted β_3 (blue dots) and $\beta_1 - 2\beta_3/3$ (red squares) from the PADs at $E = 0.2$ a.u. with δ from 0 to 2π with a step size of $\pi/4$. Solid curves are the corresponding fitting, respectively. (d) The extracted σ_{ps} (blue squares), σ_{pd} (red dots) from the β parameters. Analytical Coulomb phase differences Δ_{ps} (blue dashed curve), Δ_{pd} (red solid curve) are also presented for comparison.

phase of $\tilde{a}(t)$. The two-photon ionization pathway is modulated as a combination of the flopping to the $|\psi_b\rangle$ state and the subsequent ionization by one ω photon. Considering this, the two-photon pathway is strongly influenced by $\tilde{b}(t)$. The interference between different partial waves enables us to investigate the phases of the complex amplitudes of the two resonant states.

A. Phase extraction for the nonresonant case

We first apply the nonresonant ω - 2ω pair to a hydrogen atom with $\omega = 0.35$ a.u. The intensities are set to be $I_\omega = 1 \times 10^{13}$ W/cm 2 and $I_{2\omega} = 2.3 \times 10^{11}$ W/cm 2 , respectively, which lie well within the perturbative region. The ground-state depletion and ac-Stark shift can be safely neglected. The FWHM of both pulses are $\tau = 15.1$ fs. Figure 2(a) shows the angle-resolved PMD for $\delta = 0$. Strong left-right asymmetry can be seen, which is caused by the interference between different partial waves. The PAD is extracted from the PMD at the $E = 0.2$ a.u., as shown in Fig. 2(b) for $\delta = 0$. By scanning the relative phase δ of the two pulses from 0 to 2π , we obtain a series of PADs, from which the β parameters can be obtained, as displayed in Fig. 2(c). Figure 2(d) shows the extracted σ_{ps} and σ_{pd} from the β parameters at different photoelectron energies near the peak $E = 0.2$ a.u.

In this nonresonant case, the phase of each partial wave in hydrogen atoms, excluding the centrifugal potential phase, is trivially the same as the analytical Coulomb phase shift. This is confirmed by the comparison of the TDSE results with the analytical ones, as shown in Fig. 2(d). One can see that the extracted results, $\sigma_{pd} = 0.67$ and $\sigma_{ps} = -1.00$, are in line with $\Delta_{pd} = \Delta_p - \Delta_d$ and $\Delta_{ps} = \Delta_p - \Delta_s$, respectively. Δ_s , Δ_p ,

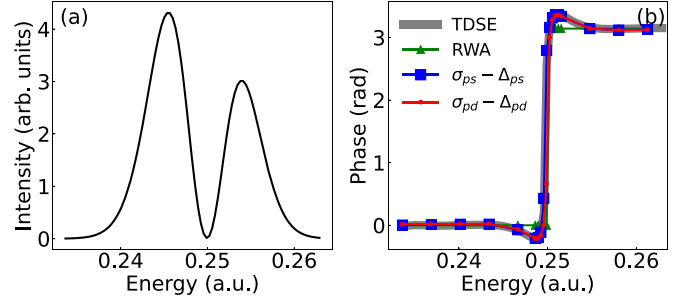


FIG. 3. (a) The angle-integrated PES for $\omega = 0.375$ a.u., $I_\omega = 1 \times 10^{13}$ W/cm 2 , $I_{2\omega} = 2.3 \times 10^{11}$ W/cm 2 , $\delta = 0$, and $\tau = 15.1$ fs. (b) $\Delta\theta(E)$ extracted from the β parameters, from both σ_{ps} (blue squares) and σ_{pd} (red dots), respectively. Results obtained from perturbation theory, where $\tilde{a}(t)$ and $\tilde{b}(t)$ obtained under the RWA (green triangles) and from the TDSE simulation (bold gray curve) are applied, are also shown. The Rabi oscillation manifests itself as a π phase jump at $E = 0.25$ a.u.

and Δ_d are the Coulomb phase shifts calculated analytically by Eq. (9). For more complex atoms or molecules, when the analytical results are not available, the ω - 2ω photoionization method provides a feasible way to measure the phase difference between one- and two-photon transition amplitudes, as well as the Wigner delay difference of the partial waves [37].

B. π phase jump in extracted phase-shift difference

To induce the Rabi oscillation between the $1s$ and $2p$ states, ω is tuned to 0.375 a.u. The transition dipole z_{ab} between the two states of hydrogen atoms is $128\sqrt{2}/243$ [24]. We set the laser parameters to $I_\omega = 1 \times 10^{13}$ W/cm 2 , $I_{2\omega} = 2.3 \times 10^{11}$ W/cm 2 , and $\tau = 15.1$ fs. The corresponding Rabi frequency is $w_r = E_\omega z_{ab} = 0.0126$ a.u., where E_ω is the peak electric field of the ω pulse. Since the Rabi dynamics can be strongly affected by the pulse envelope, for the Gaussian envelope used here, close to two Rabi periods are involved in this process based on the area theorem [51]. Under such circumstances, the strong oscillation between the two resonant states ensures the dominance of the contribution from one-photon ionization from the $2p$ state, rather than the contribution from two-photon ionization from the $1s$ state, in s and d waves. Therefore, we neglect the latter in the following discussion. This is in accordance with the acquired angle-integrated PES shown in Fig. 3(a). If the intensities of the one-photon and two-photon pathways for s and d waves are comparable, the asymmetry will be much larger [31].

When the Rabi oscillation is involved, an extra π phase jump is observed in the extracted partial wave phase differences σ_{ps} (blue squares) and σ_{pd} (red dots) compared to their Coulomb phase shift counterparts, as shown in Fig. 3(b). Based on perturbation theory, we demonstrate that the π phase jump is a direct consequence of the time evolution of the complex amplitudes of the two states. We take the wave packet resulted from the Rabi oscillation between states $|\psi_a\rangle$ and $|\psi_b\rangle$ as the zeroth-order solution. The zeroth-order wave packet $|\psi_0\rangle$ can be written as [31]

$$|\psi_0\rangle = \tilde{a}(t)e^{-iE_a t} |\psi_a\rangle + \tilde{b}(t)e^{-iE_b t} |\psi_b\rangle, \quad (17)$$

where E_a and E_b are the energies of states $|\psi_a\rangle$ and $|\psi_b\rangle$, respectively. For the continuum states with energy E around 0.25 a.u., by first-order perturbation, $|\psi_a\rangle$ can be coupled to the p wave term $|\psi_E^p\rangle$ through the 2ω pulse, while $|\psi_b\rangle$ can be coupled to the s and d wave term $|\psi_E^{s,d}\rangle$ through the ω pulse. The transition dipole are $d_a^p(E) = \langle \psi_E^p | \mathbf{A}_{2\omega} \cdot \nabla | \psi_a \rangle$, $d_b^{s,d}(E) = \langle \psi_E^{s,d} | \mathbf{A}_\omega \cdot \nabla | \psi_b \rangle$, respectively. The complex one-photon ionization amplitudes for different partial wave terms can therefore be written as [31,52–54]

$$W_p(E) = -d_a^p(E) \int_0^T e^{i(E-E_a)t} \sin(2\omega t - \delta) f(t) \tilde{a}(t) dt,$$

$$W_{s,d}(E) = -d_b^{s,d}(E) \int_0^T e^{i(E-E_b)t} \sin(\omega t) f(t) \tilde{b}(t) dt, \quad (18)$$

where T is the pulse duration, and $f(t)$ is the Gaussian envelope of the pulse pair. Since the Coulomb phase shifts are offered by the terms $\langle \psi_E^p | \mathbf{A}_{2\omega} \cdot \nabla | \psi_a \rangle$ and $\langle \psi_E^{s,d} | \mathbf{A}_\omega \cdot \nabla | \psi_b \rangle$, the extra phase jump is attributed to the integral kernel. The phase of the laser field δ can be taken out just as Eq. (10). The remaining integration can be viewed as a Fourier transformation of the phases of the two resonant states from the time domain to the energy domain

$$\theta_a(E) = \arg \left[\int_0^T e^{i(E-E_a)t} \sin(2\omega t) f(t) \tilde{a}(t) dt \right],$$

$$\theta_b(E) = \arg \left[\int_0^T e^{i(E-E_b)t} \sin(\omega t) f(t) \tilde{b}(t) dt \right]. \quad (19)$$

The partial wave phases can now be written as $\sigma_p(E) = \Delta_p(E) + \theta_a(E)$ and $\sigma_{s,d}(E) = \Delta_{s,d}(E) + \theta_b(E)$. If the amplitudes $|\tilde{a}(t)| = |\tilde{b}(t)| = 1$ and the phases $\Theta_a(t) = \Theta_b(t) = 0$, the integral kernels in Eq. (19) are positive pure imaginary numbers under the rotating wave approximation (RWA) [55] due to the symmetry of the functions with respect to $T/2$ [53]. $\theta_a(E)$ and $\theta_b(E)$ will cancel each other out. However, in the case of Rabi oscillations, the amplitudes and the extra phases of the two resonant states will result in a phase-shift difference $\Delta\theta(E)$ between the two states. It will then be reflected in the deviation of the partial wave difference from the one calculated by the Coulomb phase shifts, namely,

$$\Delta\theta(E) = \theta_a(E) - \theta_b(E) = \sigma_{pd}(E) - \Delta_{pd}(E). \quad (20)$$

In other words, the phase information that we extract in Fig. 3(b) represents the phase-shift difference between the two resonant states.

To further confirm our analysis, we examine the analytical expressions for $\tilde{a}(t)$ and $\tilde{b}(t)$ under the RWA. If we only focus on the ω component of the laser field and ignore the effect of the envelope, $\tilde{a}(t)$ and $\tilde{b}(t)$ can be directly solved with the initial condition $\tilde{a}(0) = 1$ and $\tilde{b}(0) = 0$ as [31]

$$\tilde{a}(t) = \left[\cos\left(\frac{Wt}{2}\right) - i \frac{\Delta\omega}{W} \sin\left(\frac{Wt}{2}\right) \right] e^{i\Delta\omega t/2},$$

$$\tilde{b}(t) = i \frac{\omega_r}{W} \sin\left(\frac{Wt}{2}\right) e^{-i\Delta\omega t/2}, \quad (21)$$

where $\Delta\omega = \omega - (E_b - E_a)$ and $W = \sqrt{\omega_r^2 + \Delta\omega^2}$ is the generalized Rabi frequency. From Eqs. (19) and (20), the phase difference of the two resonant states can be calculated as

$$\Delta\theta(E) = \arg \left[\frac{i}{2} \int_0^{T'} e^{i(E-E_a-2\omega t)} \cos\left(\frac{Wt}{2}\right) dt \right]$$

$$- \arg \left[-\frac{1}{2} \int_0^{T'} e^{i(E-E_b-\omega t)} \sin\left(\frac{Wt}{2}\right) dt \right], \quad (22)$$

where T' is set to be two Rabi periods, as determined by the area theorem, to approximate the case with the Gaussian envelope in the TDSE calculation. The result is an abrupt phase jump at $E = 0.25$ a.u., as shown by the green triangles in Fig. 3(b). To cover the effect of the envelope, which varies the Rabi frequency from time to time, we directly incorporate the $\tilde{a}(t)$ and $\tilde{b}(t)$ obtained from the TDSE calculation into Eq. (19). The resulting curve is depicted as the bold gray curve in Fig. 3(b), which is consistent with the one fitted from the β parameters. From the above results, we can consider such a π phase jump as the fingerprint of Rabi dynamics concealed in the angle-resolved PMD.

C. Phase difference information in the time domain

When multiple Rabi periods are involved in the process, there are multiple ionization channels for each of the resonant states in the time domain. The interference of different channels manifests itself as the splitting of the two resonant states, which ultimately results in the formation of an AT-doublet in the PES. From Eq. (21), in the resonant case ($\Delta\omega = 0$), the splitting of each state occurs when the signs of $\tilde{a}(t)$ and $\tilde{b}(t)$ change, respectively. This is accompanied by a π phase jump in the time domain. The splitting of the $|\psi_a\rangle$ state occurs half a Rabi period ahead of the $|\psi_b\rangle$ state. To identify the different stages of Rabi dynamics, we further investigate the characteristics of the phase difference $\Delta\theta$ in the energy space by controlling the pulse width. This allows us to limit the Rabi periods involved in the entire process. In addition, to distinguish the contributions from the amplitudes and phases of the two states, $|\tilde{a}(t)|$ and $|\tilde{b}(t)|$ are also applied to Eq. (19).

As a result of the envelope effect, the Rabi frequency varies with the field strength, $E(t)$. Therefore, the Rabi periods involved in the process should be estimated using the area theorem and the populations of the two resonant states. Figure 4(a) shows the populations of the $1s$ and $2p$ states for the case of $\tau = 3.7$ fs, which indicates that the process contains less than 1 Rabi period. In this case, each of the s , d , and p wave pathways has only one ionization channel in the time domain. As a result, instead of the occurrence of a sudden π phase jump, $\Delta\theta$ decreases monotonically with respect to E , as shown in Fig. 4(b). Figure 4(c) shows the $\Delta\theta$, θ_a , and θ_b calculated from Eq. (19) by exerting $\tilde{a}(t)$, $\tilde{b}(t)$ from the TDSE calculation. Since only the phase difference and the trend of change are meaningful, to better display the results, θ_a and θ_b are shown in the reference where the starting point of θ_a in the figure is 0. All the following pictures with the same curves follow this rule. While in Fig. 4(d), the $\Delta\theta$, θ_a , and θ_b are acquired through the same approach as Fig. 4(c) but the applied $\tilde{a}(t)$ and $\tilde{b}(t)$ are deprived of the extra phase terms $\Theta_a(t)$ and $\Theta_b(t)$. In other words, in this case, only the

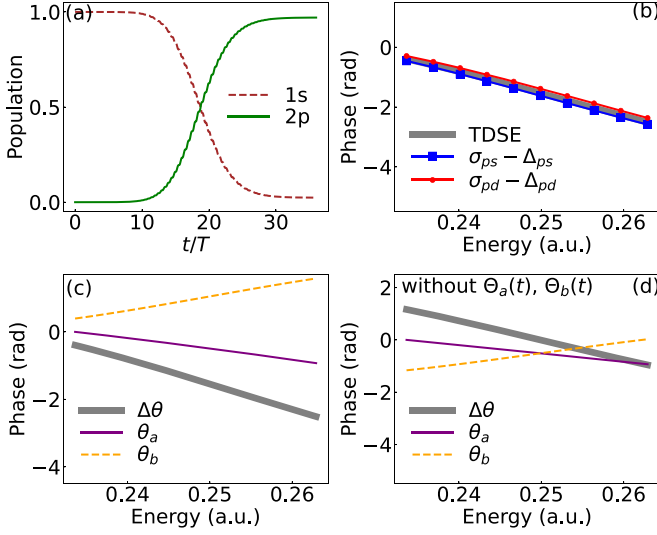


FIG. 4. (a) The populations of the $1s$ (red dashed curve) and $2p$ (green solid curve) states with laser parameters $\omega = 0.375$ a.u., $I_\omega = 1 \times 10^{13}$ W/cm 2 , $I_{2\omega} = 2.3 \times 10^{11}$ W/cm 2 , and $\tau = 3.7$ fs. (b) Same as Fig. 3(b) but for shorter pulse duration. (c) θ_a (solid purple curve) and θ_b (dashed yellow curve), together with their difference $\Delta\theta$ (bold gray curve) obtained from perturbation theory by using $\tilde{a}(t)$ and $\tilde{b}(t)$ from the TDSE calculation. (d) $\Delta\theta$, θ_a , and θ_b calculated from perturbation theory by substituting $|\tilde{a}(t)|$ and $|\tilde{b}(t)|$ from the TDSE calculation.

effect of the amplitude is considered. By comparing these two cases, it is discovered that the decrease originates from the amplitudes of the two states, while the additional phases only shift the phase of the $|\psi_b\rangle$ state by $\pi/2$. It is worth noting here that Grum-Grzhimailo *et al.* conducted a study on the PAD of hydrogen atoms using an ω - 2ω pulse pair under similar laser conditions [40]. Their investigation revealed that the degree of left-right asymmetry varies in a manner akin to a Fano-like profile with respect to the applied ω frequency. To complement their findings, they employed both first- and second-order perturbation theories starting from the initial state $|\psi_a\rangle$ to attempt to match the results derived from the TDSE calculations. The perturbation theory performed well in situations where Rabi oscillations were absent. However, the accuracy of this approach diminished when roughly half Rabi period was involved. Even in cases where only population inversion occurred at the specific pulse width, the influence of Rabi oscillations remained notably significant.

As for the case of $\tau = 8.9$ fs, 1–1.5 Rabi periods are involved in the process. Figure 5 shows the populations of the two resonant states, $\Delta\theta$, θ_a , and θ_b for $\tau = 8.9$ fs. Similar to the case shown in Fig. 3(b), $\Delta\theta$ exhibits a π phase jump. From Figs. 5(c) and 5(d), it is discovered that the jump mainly stems from the $|\psi_a\rangle$ state pathway, which is in accord with the two channels of the $|\psi_a\rangle$ state pathway and the only one channel of the $|\psi_b\rangle$ state pathway in the time domain. In addition, the population flopping, which produces two ionization channels for the $|\psi_a\rangle$ state, can lead to two phase jumps, but the phase shift will combine them into one jump located at the center of two jumps. Similar to the previous case, the $|\psi_b\rangle$ state with one channel is affected by an approximate π phase shift due to the extra phases.

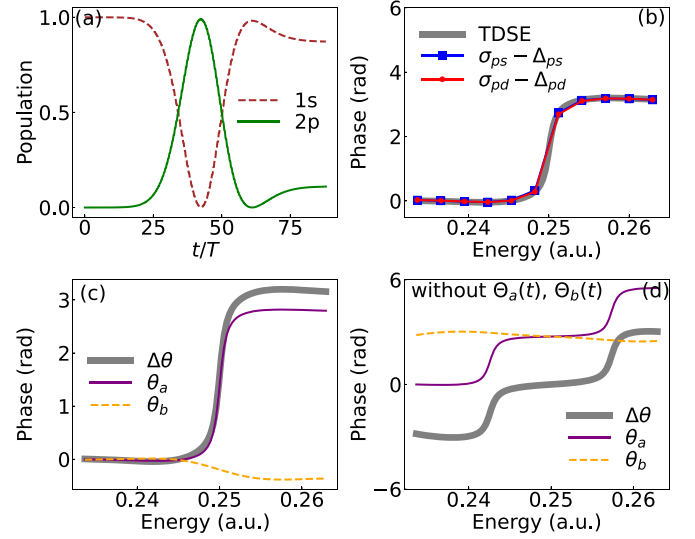


FIG. 5. Same as Fig. 4 but for $\tau = 8.9$ fs.

Figures 6(a) and 6(c) show the population information, $\Delta\theta$, θ_a , and θ_b for laser fields with $\tau = 15$ fs (1.5–2 Rabi periods) and Figs. 6(b) and 6(d) show the corresponding terms for $\tau = 16.6$ fs (more than two Rabi periods). The first is almost the same as the case in Fig. 3. In this case, both of the ionization pathways have multiple channels in the time domain. From the dominance of the $|\psi_b\rangle$ state pathway, it can be inferred that the pathway corresponding to the last ionization channel will take the lead of the phase jump. As for the latter case, the more complicated π phase up-and-down is attributed to the interference of the three channels of the $|\psi_a\rangle$ state.

D. Rabi oscillations with detuning

From Eq. (21), Rabi oscillations also emerge when the laser frequency applied is red or blue shifted from the resonant

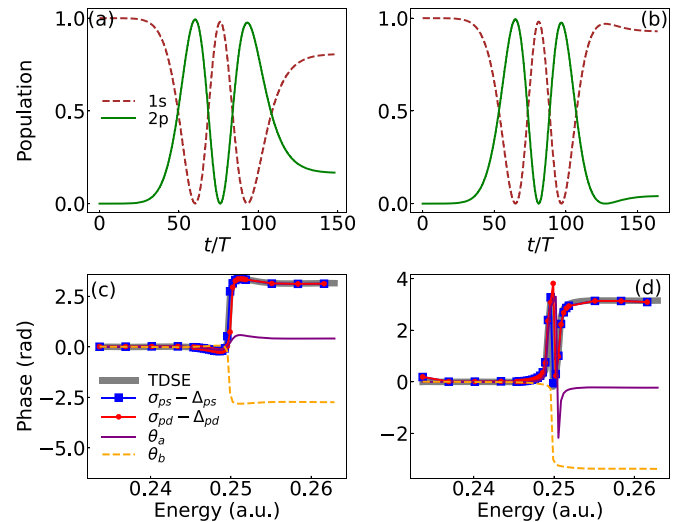


FIG. 6. (a), (b) The populations of $1s$ and $2p$ states for pulses with $\tau = 15$ (1.5–2 Rabi periods), 16.6 fs (more than two Rabi periods), respectively. (c), (d) The extracted $\Delta\theta$ and θ_a , θ_b from $\tilde{a}(t)$ and $\tilde{b}(t)$.

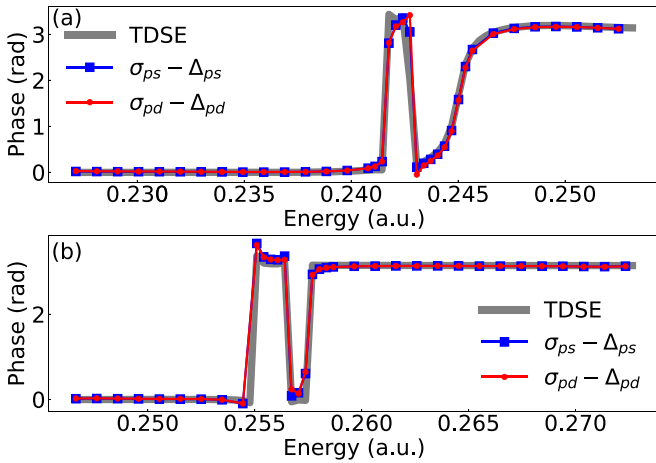


FIG. 7. Extracted $\Delta\theta$ for pulse pairs with (a) $\omega = 0.37$ a.u. (b) $\omega = 0.38$ a.u. Other laser parameters are $I_\omega = 1 \times 10^{13}$ W/cm², $I_{2\omega} = 2.3 \times 10^{11}$ W/cm², and $\tau = 15.1$ fs.

frequency. To extend our scheme to a broader frequency range that allows for general Rabi oscillation, we conduct further research on near-resonant cases. We utilize the laser with $\omega = 0.37$ a.u. and $\omega = 0.38$ a.u. to study the case for red and blue detuning, respectively. The FWHM and intensities of the ω - 2ω pairs applied in both cases are the same as the resonant one. Figures 7(a) and 7(b) show the extracted $\Delta\theta$ for $\omega = 0.37$ a.u. and $\omega = 0.38$ a.u., respectively. The more complicated $\tilde{a}(t)$ and $\tilde{b}(t)$ are reflected by multiple phase jumps in the energy space.

Differing from the resonant case, the expected π phase jump is shifted from the expected energy. For the lower laser frequency, the hopping energy is blue-detuned, while for the higher laser frequency, the hopping energy is red-detuned. The deviation from the expected ionization peak is roughly the same as $\Delta\omega$. In addition, an additional π phase jump-on-and-off occurs before or after the original phase jump in each case. In both cases, the results are consistent with the TDSE calculation. This feature cannot be well described by the analytical result, as it is influenced by the strong modulation of the envelope.

To identify the contributions from the $|\psi_a\rangle$ and $|\psi_b\rangle$ state pathways, as well as the contributions from the amplitudes and phases, we use the same approach as described in Sec. III C. It was discovered that the jump-on-and-off mainly originates from the $|\psi_a\rangle$ state pathway. Although the pulse width in this case is set the same as the one in Figs. 6(a) and 6(c), the population flopping is more subtle in near-resonant cases. As a result, unlike the resonant case, the population of the $1s$ state almost reaches 1 at the end of the pulse, creating a new channel similar to the case shown in Figs. 6(b) and 6(d). By distinguishing between the effects of the amplitudes and

phases, we find that, when considering only the effect of the amplitudes, the case exhibits normal features similar to the resonant case. Therefore, the contributions from the perturbed phase dominate. These features in the near-resonant cases are influenced by the combined effects of multiple ionization channels and phase shifts.

IV. CONCLUSION

In summary, we propose a scheme to extract the phase-shift difference induced by Rabi oscillations in the energy domain of the two resonant states from the PAD by utilizing the ω - 2ω pulse pair. The phase-shift difference is equal to the extracted partial wave phase difference minus the difference of the Coulomb phase shifts. The latter is analytical for hydrogen atoms. Compared to nonresonant cases, Rabi oscillations introduce an additional π phase jump at the expected energy in the phase difference. The result is verified by comparing the analytical solution with the one obtained directly from the TDSE calculations.

Furthermore, the number of Rabi periods involved in the process also affects the phase jump. The phase jump occurs for the ionization pathway of each state only when two channels exist for the state in the time domain. If more than three channels are included, the phase will undergo three hops. For the near-resonant cases, the energy at which the phase jump occurs is shifted in the opposite direction to the detuned laser frequency, resulting in an additional π phase jump-on-and-off. It is worth noting that the phase characteristics in all of these scenarios stem from the combined effects of the amplitudes and phases of the two resonant states.

Based on these findings, we can identify a distinct signature of Rabi dynamics encoded in the photoelectron signal. This signature, complementing the AT doublet, provides a direct insight into the intricate complex amplitudes of the two resonant states. In this context, the π phase shift serves as a more pronounced indicator of the “oscillatory” nature of Rabi dynamics. The current ω - 2ω framework has the potential to be extended and implemented with other complex atoms or molecules, as long as we can efficiently and coherently modulate the populations of bound states using a free-electron laser.

ACKNOWLEDGMENTS

This work was supported by National Natural Science Foundation of China (NSFC) (Grants No. 12274294, No. 11925405, No. 11764041, and No. 12204545) and Tianshan Talent Program of Xinjiang, China. The computations in this paper were run on the π 2.0 cluster supported by the Center for High Performance Computing at Shanghai Jiao Tong University. We thank Xu Zhang and Yueming Zhou for helpful discussions regarding this work.

- [1] I. I. Rabi, *Phys. Rev.* **51**, 652 (1937).
- [2] T. R. Gentile, B. J. Hughey, D. Kleppner, and T. W. Ducas, *Phys. Rev. A* **40**, 5103 (1989).
- [3] S. T. Cundiff, A. Knorr, J. Feldmann, S. W. Koch, E. O. Göbel, and H. Nickel, *Phys. Rev. Lett.* **73**, 1178 (1994).

- [4] A. A. Batista and D. S. Citrin, *Phys. Rev. Lett.* **92**, 127404 (2004).
- [5] V. V. Albert, *Phys. Rev. Lett.* **108**, 180401 (2012).
- [6] M. Fushitani, C. N. Liu, A. Matsuda, T. Endo, Y. Toida, M. Nagasono, T. Togashi, M. Yabashi, T. Ishikawa, Y. Hikosaka,

- T. Morishita, and A. Hishikawa, *Nat. Photonics* **10**, 102 (2016).
- [7] M. Saffman, T. G. Walker, and K. Mølmer, *Rev. Mod. Phys.* **82**, 2313 (2010).
- [8] K. Bergmann, H. Theuer, and B. W. Shore, *Rev. Mod. Phys.* **70**, 1003 (1998).
- [9] M. D. Lukin, *Rev. Mod. Phys.* **75**, 457 (2003).
- [10] A. Feist, K. E. Echternkamp, J. Schauss, S. V. Yalunin, S. Schäfer, and C. Ropers, *Nature (London)* **521**, 200 (2015).
- [11] R. Vijay, C. Macklin, D. H. Slichter, S. J. Weber, K. W. Murch, R. Naik, A. N. Korotkov, and I. Siddiqi, *Nature (London)* **490**, 77 (2012).
- [12] T. H. Stievater, X. Li, D. G. Steel, D. Gammon, D. S. Katzer, D. Park, C. Piermarocchi, and L. J. Sham, *Phys. Rev. Lett.* **87**, 133603 (2001).
- [13] D. B. Milošević, B. Fetić, and P. Ranitovic, *Phys. Rev. A* **106**, 013109 (2022).
- [14] S. Pan, C. Hu, W. Zhang, Z. Zhang, L. Zhou, C. Lu, P. Lu, H. Ni, J. Wu, and F. He, *Light Sci. Appl.* **12**, 35 (2023).
- [15] C.-X. Hu, W.-Z. Li, W.-B. Zhang, X.-C. Gong, J. Wu, and F. He, *Phys. Rev. A* **103**, 043122 (2021).
- [16] S. H. Autler and C. H. Townes, *Phys. Rev.* **100**, 703 (1955).
- [17] M. Wu, S. Chen, S. Camp, K. J. Schafer, and M. B. Gaarde, *J. Phys. B* **49**, 062003 (2016).
- [18] X. Wu, Z. Yang, S. Zhang, X. Ma, J. Liu, and D. Ye, *Phys. Rev. A* **103**, L061102 (2021).
- [19] V. Stooß, S. M. Cavaletto, S. Donsa, A. Blättermann, P. Birk, C. H. Keitel, I. Březinová, J. Burgdörfer, C. Ott, and T. Pfeifer, *Phys. Rev. Lett.* **121**, 173005 (2018).
- [20] M. Anand, S. Pabst, O. Kwon, and D. E. Kim, *Phys. Rev. A* **95**, 053420 (2017).
- [21] M. Chini, X. Wang, Y. Cheng, Y. Wu, D. Zhao, D. A. Telnov, S.-I. Chu, and Z. Chang, *Sci. Rep.* **3**, 1105 (2013).
- [22] C. Ott, A. Kaldun, L. Argenti, P. Raith, K. Meyer, M. Laux, Y. Zhang, A. Blättermann, S. Hagstotz, T. Ding, R. Heck, J. Madroñero, F. Martín, and T. Pfeifer, *Nature (London)* **516**, 374 (2014).
- [23] K. Nasiri Avanaki, D. A. Telnov, and Shih-I Chu, *Phys. Rev. A* **94**, 053410 (2016).
- [24] W.-C. Jiang, H. Liang, S. Wang, L.-Y. Peng, and J. Burgdörfer, *Phys. Rev. Res.* **3**, L032052 (2021).
- [25] C. Yu and L. B. Madsen, *Phys. Rev. A* **98**, 033404 (2018).
- [26] A. Tóth and A. Csehi, *J. Phys. B* **54**, 035005 (2021).
- [27] B. Walker, M. Kaluža, B. Sheehy, P. Agostini, and L. F. DiMauro, *Phys. Rev. Lett.* **75**, 633 (1995).
- [28] L. Young, K. Ueda, M. Gühr, P. H. Bucksbaum, M. Simon, S. Mukamel, N. Rohringer, K. C. Prince, C. Masciovecchio, M. Meyer, A. Rudenko, D. Rolles, C. Bostedt, M. Fuchs, D. A. Reis, R. Santra, H. Kapteyn, M. Murnane, H. Ibrahim, F. Légaré *et al.*, *J. Phys. B* **51**, 032003 (2018).
- [29] E. Allaria, R. Appio, L. Badano, W. A. Barletta, S. Bassanese, S. G. Biedron, A. Borga, E. Busetto, D. Castronovo, P. Cinquegrana, S. Cleva, D. Cocco, M. Cornacchia, P. Craievich, I. Cudin, G. D’Auria, M. Dal Forno, M. B. Danailov, R. De Monte, G. De Ninno *et al.*, *Nat. Photonics* **6**, 699 (2012).
- [30] J. Liang, Y. Zhou, Y. Liao, W.-C. Jiang, M. Li, and P. Lu, *Ultrafast Sci.* **2022**, 9842716 (2022).
- [31] S. Nandi, E. Olofsson, M. Bertolino, S. Carlström, F. Zapata, D. Busto, C. Callegari, M. Di Fraia, P. Eng-Johnsson, R. Feifel, G. Gallician, M. Gisselbrecht, S. Maclot, L. Neoričić, J. Peschel, O. Plekan, K. C. Prince, R. J. Squibb, S. Zhong, P. V. Demekhin *et al.*, *Nature (London)* **608**, 488 (2022).
- [32] E. Lindroth, F. Calegari, L. Young, M. Harmand, N. Dudovich, N. Berrah, and O. Smirnova, *Nat. Rev. Phys.* **1**, 107 (2019).
- [33] K. C. Prince, E. Allaria, C. Callegari, R. Cucini, G. De Ninno, S. Di Mitri, B. Diviacco, E. Ferrari, P. Finetti, D. Gauthier, L. Giannessi, N. Mahne, G. Penco, O. Plekan, L. Raimondi, P. Rebernik, E. Roussel, C. Svetina, M. Trovò, M. Zangrando *et al.*, *Nat. Photonics* **10**, 176 (2016).
- [34] X. Zhang, Y. Zhou, Y. Liao, Y. Chen, J. Liang, Q. Ke, M. Li, A. Csehi, and P. Lu, *Phys. Rev. A* **106**, 063114 (2022).
- [35] J. J. Cui, Y. Cheng, X. Wang, Z. Li, N. Rohringer, V. Kimberg, and S. B. Zhang, *Phys. Rev. Lett.* **131**, 043201 (2023).
- [36] L. Giannessi, E. Allaria, K. C. Prince, C. Callegari, G. Sansone, K. Ueda, T. Morishita, C. N. Liu, A. N. Grum-Grzhimailo, E. V. Gryzlova, N. Douguet, and K. Bartschat, *Sci. Rep.* **8**, 7774 (2018).
- [37] M. Di Fraia, O. Plekan, C. Callegari, K. C. Prince, L. Giannessi, E. Allaria, L. Badano, G. De Ninno, M. Trovò, B. Diviacco, D. Gauthier, N. Mirian, G. Penco, P. R. Ribič, S. Spampinati, C. Spezzani, G. Gaio, Y. Orimo, O. Tugs, T. Sato *et al.*, *Phys. Rev. Lett.* **123**, 213904 (2019).
- [38] D. You, K. Ueda, E. V. Gryzlova, A. N. Grum-Grzhimailo, M. M. Popova, E. I. Staroselskaya, O. Tugs, Y. Orimo, T. Sato, K. L. Ishikawa, P. A. Carpeggiani, T. Csizmadia, M. Füle, G. Sansone, P. K. Maroju, A. D’Elia, T. Mazza, M. Meyer, C. Callegari, M. Di Fraia *et al.*, *Phys. Rev. X* **10**, 031070 (2020).
- [39] E. P. Wigner, *Phys. Rev.* **98**, 145 (1955).
- [40] A. N. Grum-Grzhimailo, E. V. Gryzlova, E. I. Staroselskaya, J. Venzke, and K. Bartschat, *Phys. Rev. A* **91**, 063418 (2015).
- [41] N. Douguet, E. V. Gryzlova, E. I. Staroselskaya, K. Bartschat, and A. N. Grum-Grzhimailo, *Eur. Phys. J. D* **71**, 105 (2017).
- [42] E. V. Gryzlova, A. N. Grum-Grzhimailo, E. I. Staroselskaya, N. Douguet, and K. Bartschat, *Phys. Rev. A* **97**, 013420 (2018).
- [43] E. V. Gryzlova, M. M. Popova, A. N. Grum-Grzhimailo, E. I. Staroselskaya, N. Douguet, and K. Bartschat, *Phys. Rev. A* **100**, 063417 (2019).
- [44] Z.-H. Zhang, Y. Li, Y.-J. Mao, and F. He, *Comput. Phys. Commun.* **290**, 108787 (2023).
- [45] L. B. Madsen, L. A. A. Nikolopoulos, T. K. Kjeldsen, and J. Fernández, *Phys. Rev. A* **76**, 063407 (2007).
- [46] B. Fetić, M. Tunja, W. Becker, and D. B. Milošević, *Phys. Rev. A* **105**, 053121 (2022).
- [47] B. Fetić, W. Becker, and D. B. Milošević, *Phys. Rev. A* **102**, 023101 (2020).
- [48] K. L. Ishikawa and K. Ueda, *Appl. Sci.* **3**, 189 (2013).
- [49] Y.-Y. Yin, C. Chen, D. S. Elliott, and A. V. Smith, *Phys. Rev. Lett.* **69**, 2353 (1992).
- [50] Y. Wang and C. H. Greene, *Phys. Rev. A* **103**, 053118 (2021).
- [51] J. Eberly, *Opt. Express* **2**, 173 (1998).
- [52] W.-C. Jiang, M.-X. Wang, L.-Y. Peng, and J. Burgdörfer, *Phys. Rev. A* **105**, 023104 (2022).
- [53] M. Liu, S. U. Khan, X.-Q. Wang, P.-G. Yan, and W.-C. Jiang, *New J. Phys.* **24**, 093019 (2022).
- [54] Y. Liao, Y. Zhou, L.-W. Pi, J. Liang, Q. Ke, Y. Zhao, M. Li, and P. Lu, *Phys. Rev. A* **105**, 063110 (2022).
- [55] I. I. Rabi, N. F. Ramsey, and J. Schwinger, *Rev. Mod. Phys.* **26**, 167 (1954).